Article

Discovery Medicine 2025; 37(201): 2294–2308
https://doi.org/10.24976/Discov.Med.202537201.195

PBMC-derived DECR1 Inhibits Ferroptosis of Macrophages by Activating Catalase to Confer Cardiac Protection in Septic Myocardial Injury

Wei Zhang[1], Zhizhen Lai[2], Lisha Pang[2], Muhua Dai[2], Jianbiao Meng[2,*]

[1]Department of Cardiovascular Medicine, Tongde Hospital of Zhejiang Province, 310012 Hangzhou, Zhejiang, China
[2]Department of Critical Care Medicine, Tongde Hospital of Zhejiang Province, 310012 Hangzhou, Zhejiang, China
*Correspondence: mjb1050@163.com (Jianbiao Meng)
Submitted: 2 July 2025 Revised: 13 August 2025 Accepted: 25 August 2025 Published: 20 October 2025

Background: Sepsis-induced myocardial injury, also known as septic myocardial injury (MI), significantly elevates mortality during life-threatening organ dysfunction. While 2,4-dienoyl-CoA reductase 1 (DECR1), a well-recognized gene signature in septic myocardium and blood, and catalase (CAT), which mitigates cardiac anomalies by suppressing ferroptosis, the interaction between them during septic MI pathogenesis remains unclear. Therefore, this study investigates the underlying mechanism by which DECR1 regulates catalase-mediated ferroptosis to confer cardio-protection.

Methods: We established *in vivo* septic MI rat models and *in vitro* human monocytic leukemia cells (THP-1) cell models using 10 mg/kg and 1 μg/mL lipopolysaccharide (LPS), respectively. DECR1 was overexpressed in both systems using lentiviral vectors. Rat serum and peripheral blood mononuclear cells (PBMCs) were isolated for subsequent analyses. Myocardial function was assessed through echocardiography (ejection fraction, fractional shortening). Histopathology (Hematoxylin-Eosin (H&E), Masson's trichrome), oxidative stress markers (MDA, 4-HNE) levels, and ferroptosis-related indicators (PTGS2, ACSL4) were evaluated. Furthermore, the apoptosis rate (Terminal deoxynucleotidyl-transferase-mediated dUTP-nick-end labeling (TUNEL), caspase-3) as well as levels of inflammatory markers (tumor necrosis factor-α (TNF-α), interleukin-6 (IL-6); Enzyme-linked immunosorbent assay (ELISA)) were assessed. Additionally, THP-1 ferroptosis (C11-BODIPY fluorescence), apoptosis levels (annexin V/PI), and antioxidant activities (CAT, superoxidase dismutase (SOD)) were also evaluated.

Results: In septic MI rats, DECR1 expression decreased in PBMCs, while its overexpression attenuated myocardial oxidative stress, accompanied by increased activities/expressions of CAT and SOD, reduced myocardial ferroptosis and histological anomalies, ameliorated cardiac dysfunction, and inhibited serous and myocardial inflammation and myocardial apoptosis ($p < 0.05$). Furthermore, DECR1 overexpression suppressed ferroptosis, enhanced CAT and SOD activities/expressions, and repressed apoptosis and inflammation in LPS-stimulated THP-1 cells ($p < 0.05$).

Conclusion: DECR1 deficiency in PBMCs exacerbates septic MI by promoting ferroptosis and inflammation. DECR1 overexpression activates CAT and SOD, thereby suppressing oxidative stress, macrophage ferroptosis, and apoptosis. This study is the first to demonstrate that PBMC-derived DECR1 regulates CAT activity to suppress ferroptosis and mitigate septic MI, offering a novel therapeutic approach for septic MI management.

Keywords: septic myocardial injury; 2,4-dienoyl-CoA reductase 1; peripheral blood mononuclear cells; catalase; ferroptosis

Introduction

Sepsis, a life-threatening condition caused by a dysregulated host response [1], often leads to septic myocardial injury (MI) and subsequent transient cardiac dysfunction [2]. About 28.2% of septic patients develop MI complications [3], which are linked to a poor prognosis, particularly when afterload-related cardiac performance declines below 80% [4].

Macrophages, key immune cells that circulate in the blood or reside within heart tissues, play a pivotal role in regulating tissue homeostasis following cardiac injury [5,6]. However, during septic MI, macrophages show dysfunction, characterized by abnormal immune responses where macrophages undergo improper cell death, thereby aggravating cardiac inflammation [7,8]. Ferroptosis in macrophages further enhances their inflammatory activation [9], contributing to the progression of septic cardiac dysfunction [10].

Ferroptosis, a programmed cell death characterized by iron-mediated oxidative damage to lipid membranes [11], plays a crucial role in the pathogenesis of septic MI [12]. Bioinformatics analyses have identified 6 significant biomarkers associated with genetic and cellular pathways that undergo concurrent changes in the blood and cardiac tissues of septic patients [13]. Among these

biomarkers, 2,4-dienoyl-CoA reductase 1 (DECR1), a rate-limiting mitochondrial enzyme crucial to the metabolism and transport of polyunsaturated fatty acid (PUFA) during β-oxidation [14], has been reported to be downregulated in blood samples of septic patients [13] and in models of pressure overload-induced MI [15]. Mechanistically, DECR1 deficiency promotes the accumulation of PUFA and subsequent tumor cell ferroptosis [16]. Furthermore, DECR1 has been found to mediate the remodeling of non-infarcted myocardium by modulating macrophage-driven inflammation and fatty acid metabolism [17]. Despite these valuable insights, the precise role and underlying mechanism of DECR1 in septic MI, particularly in key immune cell types, remain largely uninvestigated.

Given these observations, unlike the previous DECR1-focused studies, which primarily examined tumor cells or cardiomyocytes themselves (such as in pressure overload models), the current study aims to investigate whether DECR1 modulates myocardial inflammation and injury by regulating ferroptosis in macrophages under septic conditions. We conjectured that DECR1 may inhibit ferroptosis in macrophages, thereby dampening myocardial inflammation and alleviating septic MI.

In the present study, we established septic rat models, collected peripheral blood samples, and constructed LPS-induced septic macrophages to validate whether DECR1 derived from peripheral blood mononuclear cells (PBMCs) can ameliorate septic MI by inhibiting ferroptosis of macrophages. This approach aims to provide a new perspective for managing septic MI.

Materials and Methods

STRING Analysis

The STRING database (https://version-11-5.string-db.org/cgi/input?sessionId=bX2LTAj6I0LS&input_page_show_search=on) was used to assess interaction between DECR1 and catalase (CAT) proteins.

Experimental Animals

The design, implementation, and reporting of this study strictly adhered to the ARRIVE 2.0 guidelines (Percie du Sert *et al.* [18], 2020, PLOS Biology) to ensure transparency, reproducibility, and ethical compliance in the animal studies. Eight-month-old male Sprague-Dawley rats (n = 30, 180–250 g) were housed in specific pathogen-free laboratory metal cages under controlled conditions (22 $\pm$ 2.0 °C, 55 $\pm$ 15% humidity, and a 12-hour light/dark circadian cycle) with free access to food and water.

Animal Grouping and Lentivirus Infection

To ascertain the expression pattern of DECR1 in septic MI, rats were randomly allocated into Control and Model groups (3 rats per group) for a preliminary experiment.

Based on the preliminary findings, a subsequent mechanistic investigation was performed, in which rats were randomly assigned into Control, Model, Model+NC, and Model+DECR1 groups (6 rats per group).

Septic MI was induced in the Model groups through intraperitoneal injection of 10 mg/kg lipopolysaccharide (LPS, L3024, Sigma-Aldrich, St. Louis, MO, USA) adjusted at a concentration of 1 mg/mL in 0.9% NaCl [19]. However, rats in the Control group were injected with an equivalent volume of 0.9% NaCl following a similar procedure. After induction, the rats in the Model+DECR1/NC group were injected with lentiviruses carrying either DECR1 or a negative control (RR208399L3/PS100092, OriGene, Rockville, MD, USA) via the tail vein (1×10^8 UT/50 µL) for three consecutive days [20]. Then, 24 hours after the final lentiviral injection, all surviving rats underwent blinded echocardiography assessment to examine cardiac function, including left ventricular end-diastolic volume (LVEDV), left ventricular end-systolic volume (LVESV), left ventricular ejection fraction (LVEF), and left ventricular fractional shortening (LVFS).

Following echocardiography evaluation, rats were immediately anesthetized with 1% pentobarbital sodium injection (50 mg/kg, Sigma-Aldrich, St. Louis, MO, USA), and peripheral blood samples were collected. The blood specimens were processed as follows: one portion was used to isolate PBMCs, and the other portion was centrifuged at $\times$2000 g for 20 minutes to collect serum, which was preserved at –20 °C for fluorescent immunoassay (FIA).

Finally, the rats were euthanized through intraperitoneal injection of 1% pentobarbital sodium (200 mg/kg, Sigma-Aldrich, St. Louis, MO, USA), and the hearts were immediately excised. Myocardial tissues underwent the following three different processing: One portion of myocardial tissues was snap-frozen in liquid nitrogen and stored at –80 °C for qRT-PCR and Western blot analyses. The other portion of the myocardial tissues was fixed in 4% paraformaldehyde for histological analyses, such as Hematoxylin-Eosin (H&E) staining, uranyl acetate and lead citrate staining, Terminal deoxynucleotidyl-transferase-mediated dUTP-nick-end labeling (TUNEL) staining, and electron microscopy preparation. The third portion of myocardial tissues was homogenized for Enzyme-linked immunosorbent assay (ELISA).

Echocardiography

Echocardiography was performed by two blinded laboratory technicians after the final lentivirus injection or LPS/NaCl injection [21]. Briefly, the remaining rats in all groups were anesthetized with 3% isoflurane inhalation (PHR2874, Sigma-Aldrich, St. Louis, MO, USA) and placed on a heated platform in the left supine position. After shaving their anterior chest hair, the rats were connected to an electrocardiogram and an ultrasound machine (Vivid E9, GE Healthcare, Chicago, IL, USA) equipped with a 12-sec

heart probe at 12 MHz frequency. Cardiac systolic and diastolic functions were evaluated by determining LVEDV, LVESV, LVEF, and LVFS. To ensure accuracy, at least three cardiac cycles were recorded for each rat.

Isolation of PBMCs

PBMCs were isolated from fresh blood using Ficoll-400 gradient centrifugation (F2637, Sigma-Aldrich, St. Louis, MO, USA) according to the manufacturer's protocol and a previously described method [22]. In brief, sodium heparin anticoagulant was added to the fresh whole blood (60 mL) and diluted at a 1:1 ratio with Hank's solution (H1641, Sigma-Aldrich, St. Louis, MO, USA). The diluted blood (30 mL) was transferred to 15 mL Ficoll-400 and centrifuged at 1000 ×g for 20 minutes at 18 °C. The opaque white interface mononuclear cell layer, comprising approximately 90% lymphocytes and 10% monocytes, was collected and washed twice using RPMI 1640 medium (11875127, ThermoFisher, Waltham, MA, USA). After an additional centrifugation at 350 ×g for 10 minutes at 18 °C, the resulting pellets (PBMCs) were resuspended and cultured in RPMI 1640 medium enriched with 10% fetal bovine serum (10099158, ThermoFisher, Waltham, MA, USA) and 1% penicillin-streptomycin (15070063, ThermoFisher, Waltham, MA, USA). All cultures were routinely tested for mycoplasma contamination and found to be contamination-free.

Giemsa Staining

Monocytes isolated by centrifugation were smeared onto glass slides for Giemsa staining. The cells were initially fixed with methanol at room temperature for 10 minutes, followed by staining with the Giemsa Staining Solution (C0133-100 mL, Beyotime, Shanghai, China) at room temperature for 15 minutes. Following staining, the slides were thoroughly washed with distilled water, air-dried, and then examined under an optical microscope (BX51; Olympus Corporation, Tokyo, Japan).

Flow Cytometry

The cells were centrifuged at 2000 ×g for 20 minutes at 4 °C to remove cell debris. The resulting cell suspension was incubated with CD45-FITC (#11-0461-82, Invitrogen, Carlsbad, CA, USA) and CD11b-PE (CD11b-PE, Invitrogen, Carlsbad, CA, USA) antibodies, vortexed to mix, and kept for 30 minutes at 4 °C in the dark. Flow cytometry analysis was performed using a FACS Aria II flow cytometer (BD Biosciences, Franklin Lakes, NJ, USA). Cells were sorted based on forward and side scatter profiles, with $CD45^+$ cells selected to exclude non-hematopoietic cells, and monocytes identified by $CD11b^+$ expression.

Hematoxylin-eosin (H&E) Staining

The myocardium tissue was fixed overnight in 4% paraformaldehyde (PH0427, Phygene, Fuzhou, China), dehydrated, and cleared with xylene (X112054, Aladdin, Shanghai, China), and then embedded in paraffin (P100931, Aladdin, Shanghai, China). Then, the embedded tissues were sectioned into 5-µm-thick slices and subjected to hematoxylin-eosin (H&E) staining. In brief, sections were deparaffinized in xylene, rehydrated, and then stained with hematoxylin (HY-N0116, MedChemExpress, Monmouth Junction, NJ, USA) for 10 minutes. Following differentiation with 1% hydrochloric ethanol, the tissue sections were immersed in 1% ammonia water (67362, Sigma-Aldrich, St. Louis, MO, USA) to develop the blue coloration, and then counterstained with eosin (HY-D0505A, MedChemExpress, Monmouth Junction, NJ, USA) for 5 minutes. Finally, the sections were cleared with xylene and sealed using neutral balsam (N861409, MACKLIN, Shanghai, China). Histological observations were conducted under an optical microscope (ZEISS Primotech, Carl Zeiss, Oberkochen, Germany) at a magnification ×100.

Uranyl Acetate and Lead Citrate Staining

For ultrastructural morphometric analysis, myocardial tissues were subjected to uranyl acetate and lead citrate staining [23]. Initially, myocardial tissues were fixed with 2.5% glutaraldehyde (G105908, Aladdin, Shanghai, China) in 0.1 mol/L cacodylate buffer (S464785, pH 7.4, Aladdin, Shanghai, China) at 4 °C for 1 hour, followed by treatment with 1% osmium tetroxide (1.04119, Sigma-Aldrich, St. Louis, MO, USA) prepared in cacodylate buffer. After dehydration, tissues were treated with propylene oxide (1576945, Sigma-Aldrich, St. Louis, MO, USA) and embedded in Eponate 12 (GP18010, Araldite, Salt Lake City, UT, USA).

The embedded tissues were sectioned into 60-to-80-nm thick slices, mounted on formvar carbon-coated copper grids, and sequentially stained with uranyl acetate (C066927, CHEMISCI, Shanghai, China) and lead citrate (C105169, CHEMISCI, China) at 42 °C for 1 hour. Finally, the ultrastructural alterations were observed under a transmission electron microscope (H-800, Hitachi, Tokyo, Japan) at a magnification ×15,000.

Cell Culture

Human monocytic leukemia cells (THP-1) were obtained from Procell (CL-0233, Shanghai, China). The cells were cultured in RPMI-1640 medium (11875119, ThermoFisher, Waltham, MA, USA) supplemented with 10% fetal bovine serum (FBS; A5669801, A5669801), 0.05 mM β-Mercaptoethanol (444203, Sigma-Aldrich, St. Louis, MO, USA), and 1% penicillin-streptomycin (TMS-AB2, Sigma-Aldrich, St. Louis, MO, USA). The cell cultures were maintained at 37 °C in a humidified atmosphere containing 5% CO_2. The cells were authenticated using STR profiling and tested to be mycoplasma-free.

Cell Transfection

DECR1 Overexpression plasmids were synthesized using full-length cDNA of DECR1 (**Supplementary File 1**) cloned into pcDNA3.1 vectors (V79520, ThermoFisher, Waltham, MA, USA). However, an empty pcDNA3.1 vector served as the negative control (NC). THP-1 cells were transfected with DECR1 overexpression plasmids/NC using Lipofectamine 3000 transfection reagent (L3000015, ThermoFisher, Waltham, MA, USA). For this purpose, cells were seeded in 96-well plates at a density of 1×10^4 cells/well and cultured until they achieved 80% confluency. For transfection, 0.3 µL Lipofectamine 3000 reagent and 0.2 µg plasmid were each diluted in 20 µL Opti-Minimal Essential Medium (MEM), thoroughly mixed and incubated at 37 °C for 15 minutes to produce gene-lipid complexes. These complexes were then added to the cells and incubated for 48 hours at 37 °C to allow transfection.

Stimulation With LPS

Both transfected and non-transfected THP-1 cells were incubated in complete culture medium containing 1 µg/mL LPS (L5293, Sigma-Aldrich, St. Louis, MO, USA) at 37 °C for 24 hours to induce *in vitro* septic models [24].

Quantitative Reverse Transcription-polymerase Chain Reaction (QRT-PCR)

Total RNA was extracted from PBMCs, myocardium, and both transfected and non-transfected THP-1 cells (with or without LPS stimulation) using Trizol reagent (15596026, ThermoFisher, Waltham, MA, USA). RNA was quantified using a spectrophotometer (NanoDrop ND-1000, ThermoFisher, Waltham, MA, USA), and subsequently, 1 µg of the total RNA was reverse-transcribed into cDNA with a cDNA synthesis kit (DRR037A, Takara, Dalian, China). Quantitative real-time PCR was performed on a LightCycler 96 system (Roche Diagnostics, Basel, Switzerland) using Eastep qPCR Master Mix (LS2062, Promega, Madison, WI, USA). The thermocycling conditions were set as follows: 95 °C for 10 minutes, followed by 40 cycles of 95 °C for 30 seconds and 60 °C for 30 seconds. Glyceraldehyde-3-phosphate dehydrogenase (*GAPDH*) was used as an internal control for normalization, and relative gene expression levels were determined using the $2^{-\Delta\Delta Ct}$ method [25]. The gene-specific primers used in qRT-PCR are listed in Table 1.

Western Blot Analysis

Total protein was isolated from rat myocardium and both transfected and non-transfected THP-1 cells (with/without LPS stimulation) using RIPA Buffer (89900, ThermoFisher, Waltham, MA, USA) containing a protease inhibitor (P8215, Sigma-Aldrich, St. Louis, MO, USA). Total proteins were quantified using a BCA kit (P0010S, Beyotime, Shanghai, China). A 50 µg protein sample was resolved by electrophoresis on a 12% SDS-PAGE gel (20328ES50, Yeasen, Shanghai, China) and subsequently transferred onto PVDF membranes (P2438, Sigma-Aldrich, St. Louis, MO, USA). The membranes were then blocked with 5% non-fat dry milk at room temperature for 1 hour. The membranes were then incubated overnight at 4 °C with primary antibodies against DECR1 (ab198848, 36 kDa, 1:300, Abcam, Cambridge, UK), Glutathione peroxidase 4 (GPX4; ab125066, 17 kDa, 1:1000, Abcam, Cambridge, UK), SLC7A11 (ab175186, 55 kDa, 1:1000, Abcam, Cambridge, UK), B-cell lymphoma 2 (Bcl-2; ab194583, 26 kDa, 1:1000, Abcam, Cambridge, UK), Bcl-2-associated X protein (Bax; ab32503, 21 kDa, 1:1000, Abcam, Cambridge, UK), Cleaved Caspase 3 (#9661, 17 kDa, 1:1000, Cell signaling technology, Danvers, MA, USA), β-actin (ab8226, 42 kDa, 1:1000, Abcam, Cambridge, UK), and GAPDH (#5174, 37 kDa, 1:1000, Cell signaling technology, Danvers, MA, USA). The next day, the membranes were washed with TBST (28360, Sigma-Aldrich, St. Louis, MO, USA), followed by incubation with HRP-conjugated Goat anti-Rabbit IgG (31460, ThermoFisher, Waltham, MA, USA) or Rabbit Anti-Mouse IgG H&L (ab6728, Abcam, Cambridge, UK) secondary antibody at room temperature for 2 hours. Protein bands were developed using ECL reagent (1705061, Bio-Rad, Hercules, CA, USA), and their intensity was semi-quantified with an Imager 600 system (GE Healthcare Life Science, Pittsburgh, PA, USA).

Cell Counting Kit-8 (CCK-8) Assay

The transfected and non-transfected THP-1 cells were seeded in 96-well plates at a density of 1×10^5 cells/mL and subsequently stimulated with or without LPS. After stimulation, 10 µL CCK-8 reagent (CA1210, Solarbio, Beijing, China) was added to each well and incubated at 37 °C for 4 hours. Finally, the absorbance was measured at 450 nm using a microplate reader (iMark, Bio-Rad Laboratories, Inc., Hercules, CA, USA).

Terminal Deoxynucleotidyl-transferase-mediated dUTP Nick-end Labeling (TUNEL) Staining

TUNEL staining was performed following a previously reported protocol with minor modifications [26]. Paraffin-embedded rat myocardial tissues were sectioned, deparaffinized, rehydrated, and treated with 20 µg/mL DNase-free proteinase K (ST532, diluted in 10 mol/L Tris-HCl, pH 7.4, Beyotime, Shanghai, China) for 20 minutes, followed by two PBS washes (P2272, Sigma-Aldrich, St. Louis, MO, USA). Transfected or non-transfected cells were stimulated with or without LPS, fixed with 4% paraformaldehyde, and permeabilized with 0.3% Triton X-100 (P0097, Beyotime, Shanghai, China) for 5 minutes.

Apoptosis rate was assessed using a TUNEL staining kit (C1086, Beyotime, Shanghai, China). Briefly, a 50 µL of TUNEL reaction mixture was prepared by combining 5 µL TdT enzyme solution with 45 µL FITC-labeled dUTP solution and incubating with each sample at 37 °C for

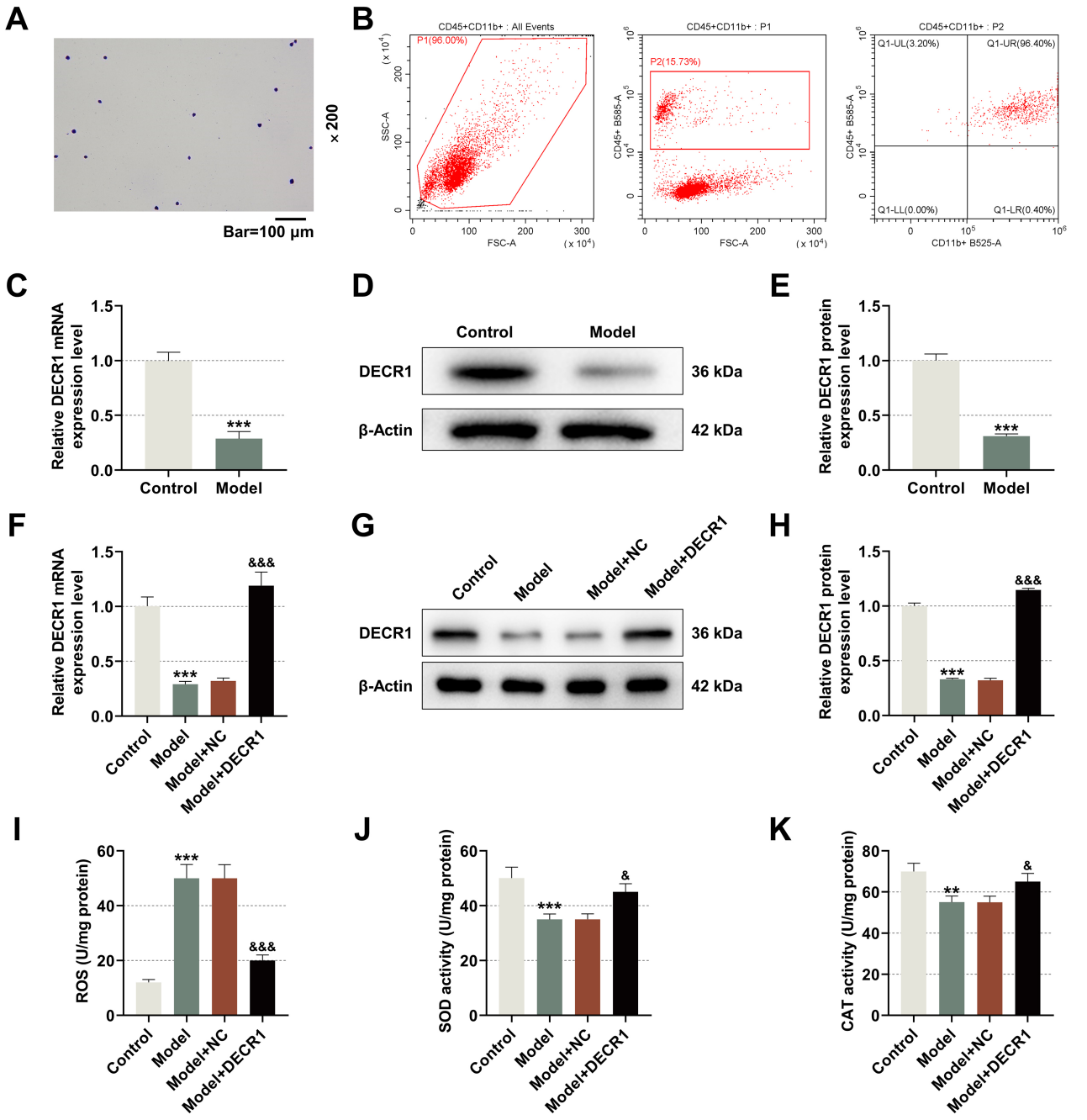

Fig. 1. *DECR1* was downregulated in PBMCs from septic MI rat models, and overexpression attenuated oxidative stress in their myocardial tissues. (A) Representative Giemsa staining of PBMCs. (B) Detection of PBMCs using flow cytometry. (C) Rats were injected intraperitoneally with 10 mg/kg LPS for 24 hours to induce septic MI, and the mRNA expression level of *DECR1* in the PBMCs was analyzed using qRT-PCR, with *β-actin* serving as an internal reference, n = 3. (D,E) DECR1 protein levels were analyzed using Western blot analysis, with β-actin as an internal reference, n = 3. (F–H) Following septic MI modeling, rats were injected with either DECR1 or NC (1×10^8 UT/50 μL) lentiviruses for three consecutive days and the expression levels of DECR1 in the PBMCs were analyzed using qRT-PCR and Western blot analysis, with β-actin serving as the internal reference. (I–K) ROS, SOD, and CAT levels in myocardial tissues were determined using ELISA. An independent *t*-test was used for comparisons between two groups, and multiple group comparisons were performed using one-way analysis of variance (ANOVA), followed by the Tukey post-hoc test, n = 3. $^{**}p < 0.01$, $^{***}p < 0.001$ vs. Control group; $^{\&}p < 0.05$, $^{\&\&\&}p < 0.001$ vs. Model+NC group. DECR1, 2,4-dienoyl-CoA reductase 1; MI, myocardial injury; PBMCs, peripheral blood mononuclear cells; NC, negative control; qRT-PCR, quantitative reverse transcription-polymerase chain reaction; ROS, reactive oxygen species; SOD, superoxidase dismutase; CAT, catalase.

Table 1. Sequences of primers used in qTR-PCR.

Genes	Species	Forward (5′-3′)	Reverse (5′-3′)
DECR1	human	TCTTCAAAAAGCGATGCTACCA	CTATCACGCACTGAGCACCT
	rats	TTTTCCAACCTCCTCTCGCC	ATGAAGTCACCCCTGCCATG
SOD1	human	GGTGGGCCAAAGGATGAAGAG	CCACAAGCCAAACGACTTCC
	rats	TAGGGAGGGAGAGGCCTAGA	CCCATTTCCTCCAGGGTGAC
SOD2	human	GCTCCGGTTTTGGGGTATCTG	GCGTTGATGTGAGGTTCCAG
	rats	ACCGAGGAGAAGTACCACGA	CCCCTGCATCGAAACAGACT
CAT	human	CGTGCTGAATGAGGAACAGA	AGTCAGGGTGGACCTCAGTG
	rats	TAACGTGTGCCTTGGAGTCC	ACTGTGTACACCAGCTGAGC
GAPDH	human	GGAGCGAGATCCCTCCAAAAT	GGCTGTTGTCATACTTCTCATGG
	rats	TGGATAGGGTGGCCGAAGTA	TACAAGGGGAGCAACAGCTG

DECR1, 2,4-dienoyl-CoA reductase 1; *SOD1*, superoxide dismutase 1; *SOD2*, superoxide dismutase 2; *CAT*, catalase; *GAPDH*, glyceraldehyde-3-phosphate dehydrogenase.

60 minutes. Cell nuclei were stained with DAPI (D9542, Sigma-Aldrich, St. Louis, MO, USA). After three PBS washes, FITC-positive cells were observed under a fluorescence microscope (Axio, Carl Zeiss, Oberkochen, Germany) at 200× and 400× magnifications. The proportion of apoptotic cells was calculated as follows: TUNEL-positive cell (%) = (number of TUNEL – positive cell nuclei/total number of nuclei) × 100.

ELISA

Myocardial tissues were homogenized in PBS, and the homogenate was centrifuged at 5000 ×g for 10 minutes to collect supernatant. Similarly, THP-1 cells (with or without transfection) were stimulated with or without LPS, followed by centrifugation at 2000 ×g for 20 minutes to obtain the supernatant.

The levels of ROS, superoxidase dismutase (SOD), and CAT in the collected supernatant, as well as interleukin-1β (IL-1β), interleukin-6 (IL-6), and tumor necrosis factor-α (TNF-α) levels in myocardial homogenate supernatant were determined using chromogenic ELISA kits (J23513, J21118, and J23625, GILED biotechnology, Wuhan, China & PI303, PI328, and PT516, Beyotime, Shanghai, China). For this purpose, diluted serum or supernatant was added to capture antibody-coated 96-well plates and was mixed thoroughly. Then, HRP-labeled antibody was added, and the plates were incubated at 37 °C for 60 minutes. The plates were washed with distilled water, and then chromogenic substrate was added and incubated for 15 minutes in the dark. The reaction was terminated using a stop solution, and the absorbance was determined at 450 nm by employing a microplate reader.

Fluorescent Immunoassay (FIA)

The levels of troponin I (TNI), heart-type fatty acid binding protein (HFABP), pro-brain natriuretic peptide (ProBNP), C-reactive protein (CRP), and procalcitonin (PCT) in rat serum, as well as the CRP and PCT levels in the supernatant of transfected or non-transfected THP-1 cells (with or without LPS stimulation), were measured using fluorescent ELISA kits. The TNI kits were customized from Abcam (UK), while kits for other biomarkers were obtained from Beyotime (P0205L, Shanghai, China). The protocol was similar to that of the chromogenic ELISA, except that the HRP-catalyzed substrate emitted fluorescent signals instead of colorimetric ones. These more sensitive fluorescent signals were detected using a fluorescence plate reader (PHERAstar FSX, BMG LABTECH, Ortenberg, Germany).

Statistical Analysis

Statistical analyses were conducted using GraphPad Prism (version 8.0, GraphPad Software Inc., San Diego, CA, USA). All data were expressed as mean ± standard deviation (SD). Data normality was evaluated using the Shapiro-Wilk test. For data that follow a normal distribution, comparisons between two groups were conducted using an independent samples *t*-test. Two-way analysis of variance (ANOVA) was used for two-variable comparisons. However, one-way ANOVA followed by the Tukey post-hoc test was applied for one-variable comparisons. Moreover, for data not following a normal distribution, the Kruskal-Wallis test was used for multiple group comparisons. Statistical significance was defined at a *p*-value of <0.05.

Results

DECR1 was Downregulated in PBMCs Obtained From Septic MI Rat Models, and Its Overexpression Attenuated Oxidative Stress in Myocardial Tissues

The purity of mononuclear cells was verified by Giemsa staining (Fig. 1A). Monocytes were further identified as a $CD45^+$ $CD11b^+$ cell population (Fig. 1B). To assess the potential role of DECR1, Septic MI rat models were established. qRT-PCR and Western blot analyses showed that DECR1 expression in PBMCs obtained from septic MI rats was significantly lower than that in control

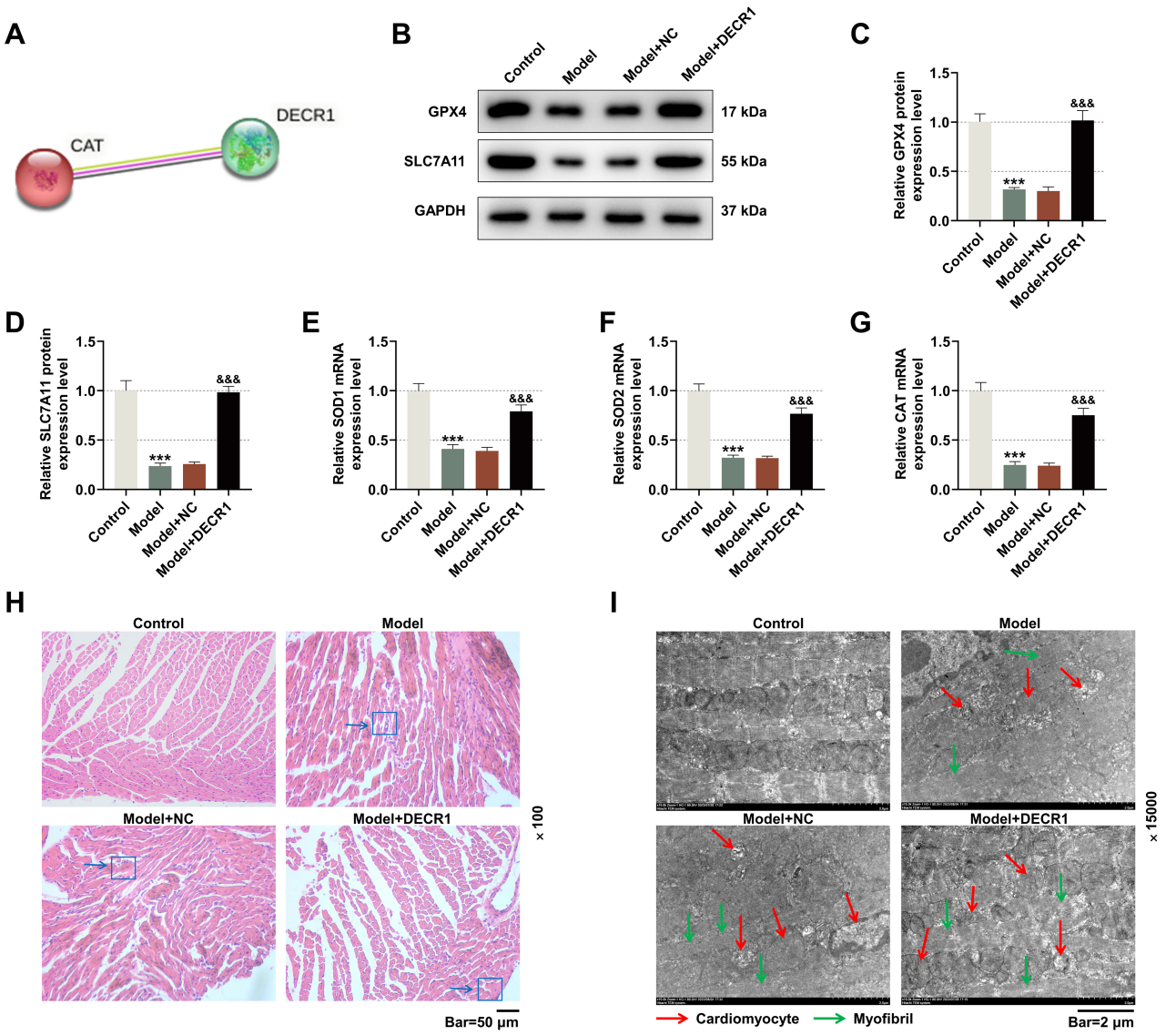

Fig. 2. *DECR1* overexpression reduced ferroptosis and alleviated histological anomalies in the myocardial tissues of septic MI rats. (A) STRING database was used for predicting DECR1 and CAT interaction. (B–D) Rats were injected intraperitoneally with 10 mg/kg LPS for 24 hours to induce septic MI and then received lentiviruses carrying DECR1/NC (1×10^8 UT/50 µL) for three consecutive days. The expression levels of GPX4 and SLC7A11 in the myocardial tissues were analyzed using Western blot analysis, with GAPDH serving as an internal reference. (E–G) The expression levels of *SOD1*, *SOD2*, and *CAT* in myocardial tissues were assessed using qRT-PCR, with *GAPDH* serving as an internal reference. (H,I) Histological examination of myocardial tissues was performed with hematoxylin-eosin staining (H) (magnification, × 100; scale bar, 50 µm) and uranyl acetate and lead citrate staining (I) (magnification, ×15,000; scale bar, 2 µm). Blue arrow: inflammatory cell infiltration and disordered myocardial fiber structure; Red arrow: Cardiomyocytes; Green arrow: Myofibrils. One-way analysis of variance (ANOVA) was applied for multiple group comparisons, followed by Tukey post-hoc analysis, n = 3. $^{***}p < 0.001$ vs. Control group; $^{\&\&\&}p < 0.001$ vs. Model+NC group. DECR1, 2,4-dienoyl-CoA reductase 1; MI, myocardial injury; NC, negative control; qRT-PCR, quantitative reverse transcription-polymerase chain reaction; GPX4, glutathione peroxidase 4; SOD1/2, superoxidase dismutase 1/2; CAT, catalase.

rats (Fig. 1C–E, $p < 0.001$). Subsequently, septic MI rats received lentivirus carrying DECR1, and both qRT-PCR and Western blot confirmed the successful transfection of DECR1 overexpression plasmids in septic MI rats-derived PBMCs (Fig. 1F–H, $p < 0.001$). Furthermore, ELISA analyses of myocardial tissues revealed elevated ROS production and reduced SOD and CAT activities in septic MI rats (Fig. 1I–K, $p < 0.01$), which were substantially reversed by *DECR1* overexpression (Fig. 1I–K, $p < 0.05$).

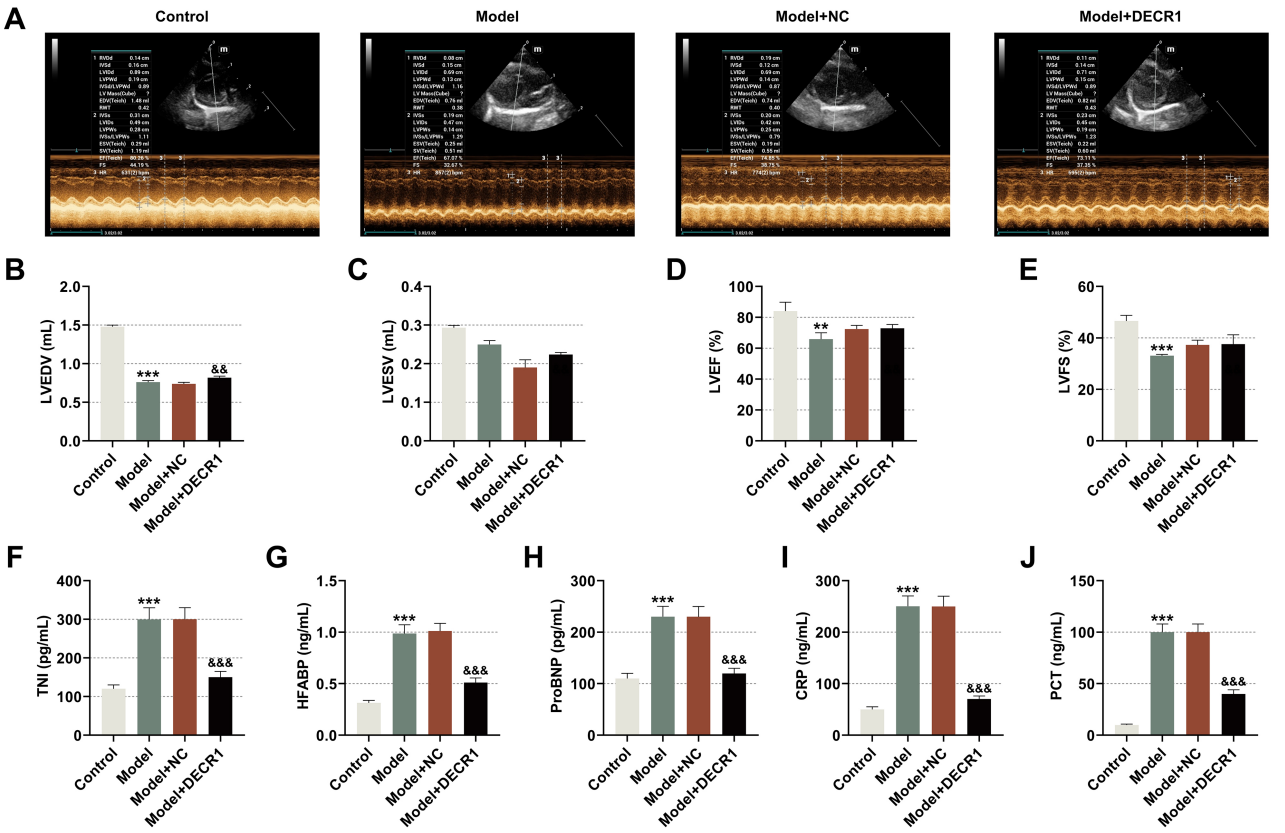

Fig. 3. *DECR1* overexpression ameliorated cardiac function and inhibited myocardial inflammation in septic MI rat models. (A–E) Rats were injected intraperitoneally with 10 mg/kg LPS for 24 hours to induce septic MI and then received lentiviruses carrying DECR1/NC (1×10^8 UT/50 µL) for three consecutive days, followed by echocardiographic assessments of cardiac function. (F–J) Serum levels of TNI, HFABP, ProBNP, CRP, and PCT were determined using fluorescent immunoassay. $^{**}p < 0.01$, $^{***}p < 0.001$ vs. Control group; $^{\&\&}p < 0.01$, $^{\&\&\&}p < 0.001$ vs. Model+NC group. DECR1, 2,4-dienoyl-CoA reductase 1; MI, myocardial injury; NC, negative control; LVEDV, left ventricular end diastolic volume; LVESV, left ventricular end systolic volume; LVEF, left ventricular ejection fraction; LVFS, left ventricular fractional shortening; TNI, troponin I; HFABP, heart-type fatty acid binding protein; ProBNP, pro-brain natriuretic peptide; CRP, C-reactive protein; PCT, procalcitonin.

DECR1 Overexpression Reduced Ferroptosis and Alleviated Histological Anomalies in the Myocardial Tissues in Septic MI Rat Models

STRING analysis indicated a potential interaction between DECR1 and CAT (Fig. 2A). The expression levels of ferroptosis-inhibiting proteins, GPX4 and SLC7A11, were significantly diminished in myocardial tissues of septic MI rats (Fig. 2B–D, $p < 0.001$), concomitant with a decline in antioxidant capacity, as evidenced by decreased *SOD1*, *SOD2*, and *CAT* mRNA levels (Fig. 2E–G, $p < 0.001$). In contrast, *DECR1* overexpression substantially elevated both these ferroptosis-inhibiting proteins and antioxidant genes (Fig. 2B–G, $p < 0.001$).

Furthermore, histological analyses also revealed myocardial injury. H&E staining demonstrated significant MI in the myocardial tissues of septic MI rats, with disorganized myocardial structure, interstitial edema, ruptured myocardial fibers, and infiltration of inflammatory cells, all of which were notably alleviated by DECR1 overexpression (Fig. 2H). Similarly, transmission electron microscopy of myocardial tissues stained with uranyl acetate and lead citrate demonstrated vacuolization and irregular swelling of cardiomyocyte mitochondria, along with partial dissolution of myofibers in the septic myocardial tissues; these alterations were substantially mitigated by DECR1 overexpression (Fig. 2I).

DECR1 Overexpression Ameliorated Cardiac Function and Inhibited Myocardial Inflammation and Apoptosis in Septic MI Rat Models

Cardiac function examination using echocardiography revealed that septic MI induction reduced LVEDV and LVESV, and decreased LVEF and LVFS in rats (Fig. 3A–E, $p < 0.01$). However, *DECR1* overexpression substantially restored LVEDV (Fig. 3A–E, $p < 0.05$), without affecting LVESV, LVEF, or LVFS (Fig. 3A–E). Furthermore, the FIA unveiled a significant upregulation in serum levels of TNI, HFABP, ProBNP, CRP, and PCT in septic MI rats

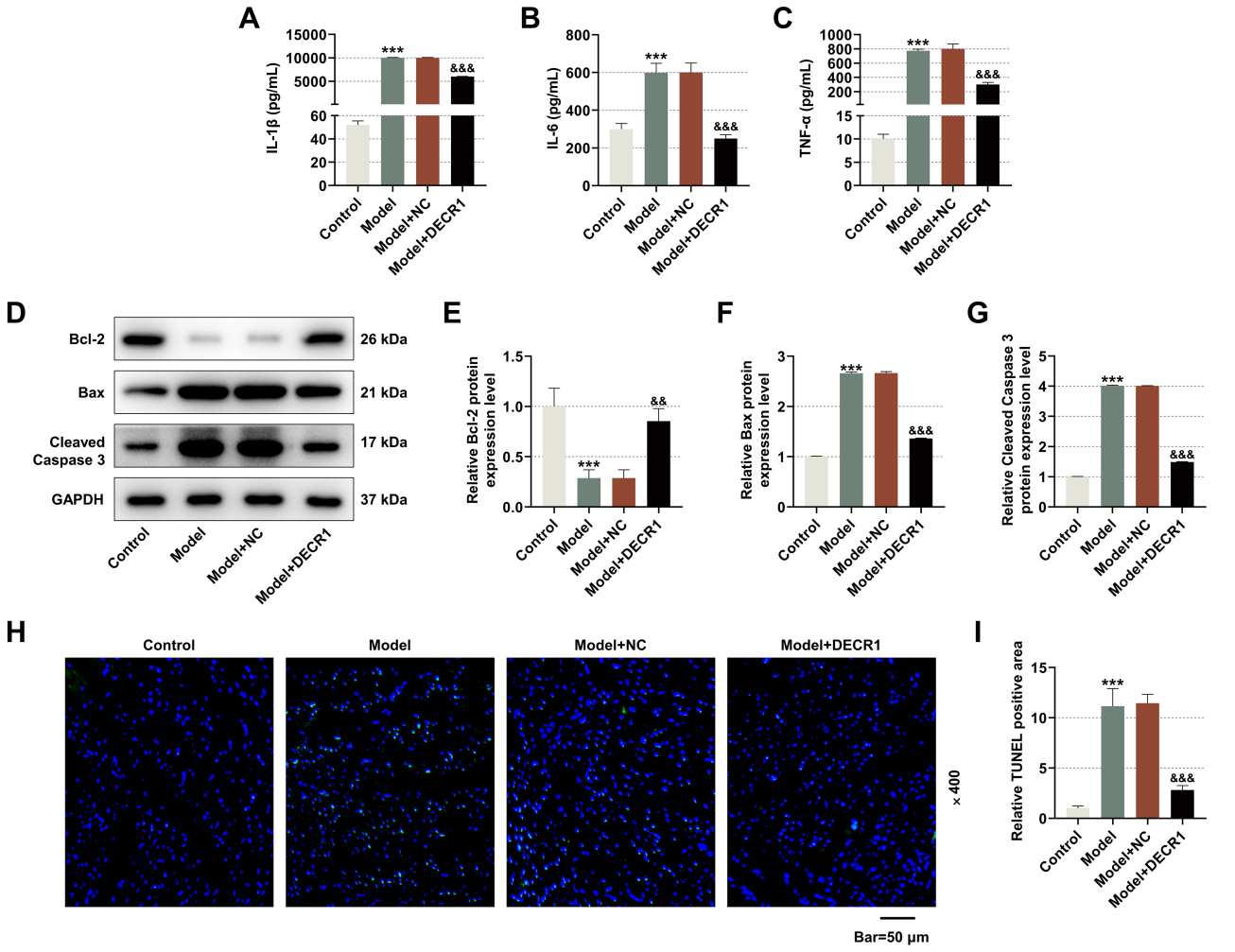

Fig. 4. *DECR1* overexpression inhibited myocardial inflammation and apoptosis in septic MI rat models. (A–C) IL-1β, IL-6, and TNF-α levels in myocardial tissues were determined using an enzyme-linked immunosorbent assay. (D–G) The expression levels of Bcl-2, Bax and Cleaved Caspase 3 in myocardial tissues were assessed using Western blot analysis, with GAPDH served as an internal reference. (H,I) Myocardial apoptosis was evaluated using TUNEL staining (magnification, ×400; scale bar, 50 μm). One-way analysis of variance (ANOVA) was used for multiple group comparisons, followed by Tukey's post-hoc test, n = 3. $^{***}p < 0.001$ vs. Control group; $^{\&\&}p < 0.01$, $^{\&\&\&}p < 0.001$ vs. Model+NC group. IL-1β, interleukin-1β; IL-6, interleukin-6; TNF-α; tumor necrosis factor-α; Bcl-2, B-cell lymphoma 2; Bax, Bcl-2-associated X protein.

(Fig. 3F–J, $p < 0.001$). Similarly, ELISA results revealed a substantial increase in IL-1β, IL-6 and TNF-α levels in septic MI rats (Fig. 4A–C, $p < 0.001$). Notably, *DECR1* overexpression significantly reduced the levels of these serum biomarkers and pro-inflammatory cytokines in septic MI rats (Fig. 3F–J,4A–C, $p < 0.001$). Additionally, Bcl-2 expression was downregulated, while Bax and Cleaved Caspase 3 levels were upregulated (Fig. 4D–G, $p < 0.01$), consistent with an increase in TUNEL-positive cardiomyocytes in septic MI rats (Fig. 4H,I, $p < 0.001$). After *DECR1* overexpression, cardiomyocyte apoptosis was substantially decreased, evidenced by reduced Bax and Cleaved Caspase-3 levels, elevated Bcl-2 expression, and fewer TUNEL-positive cells (Fig. 4D–I, $p < 0.01$).

DECR1 Overexpression Dampened Ferroptosis and Enhanced Antioxidant Capability in LPS-stimulated THP-1 Cells

LPS treatment reduced *DECR1* expression in a time-dependent manner (Fig. 5A, $p < 0.01$). When THP-1 cells were exposed to LPS to induce an *in vitro* sepsis model, DECR1 expression substantially diminished at both mRNA and protein levels compared to the control cells (Fig. 5B–D, $p < 0.001$). Transfection with the DECR1 overexpression plasmid successfully augmented DECR1 expression in LPS-exposed THP-1 cells (Fig. 5B–D, $p < 0.001$).

Furthermore, LPS exposure also resulted in increased ROS production along with reduced SOD and CAT activities (Fig. 5E–G, $p < 0.05$), effects that were attenuated by *DECR1* overexpression (Fig. 5E–G, $p < 0.05$).

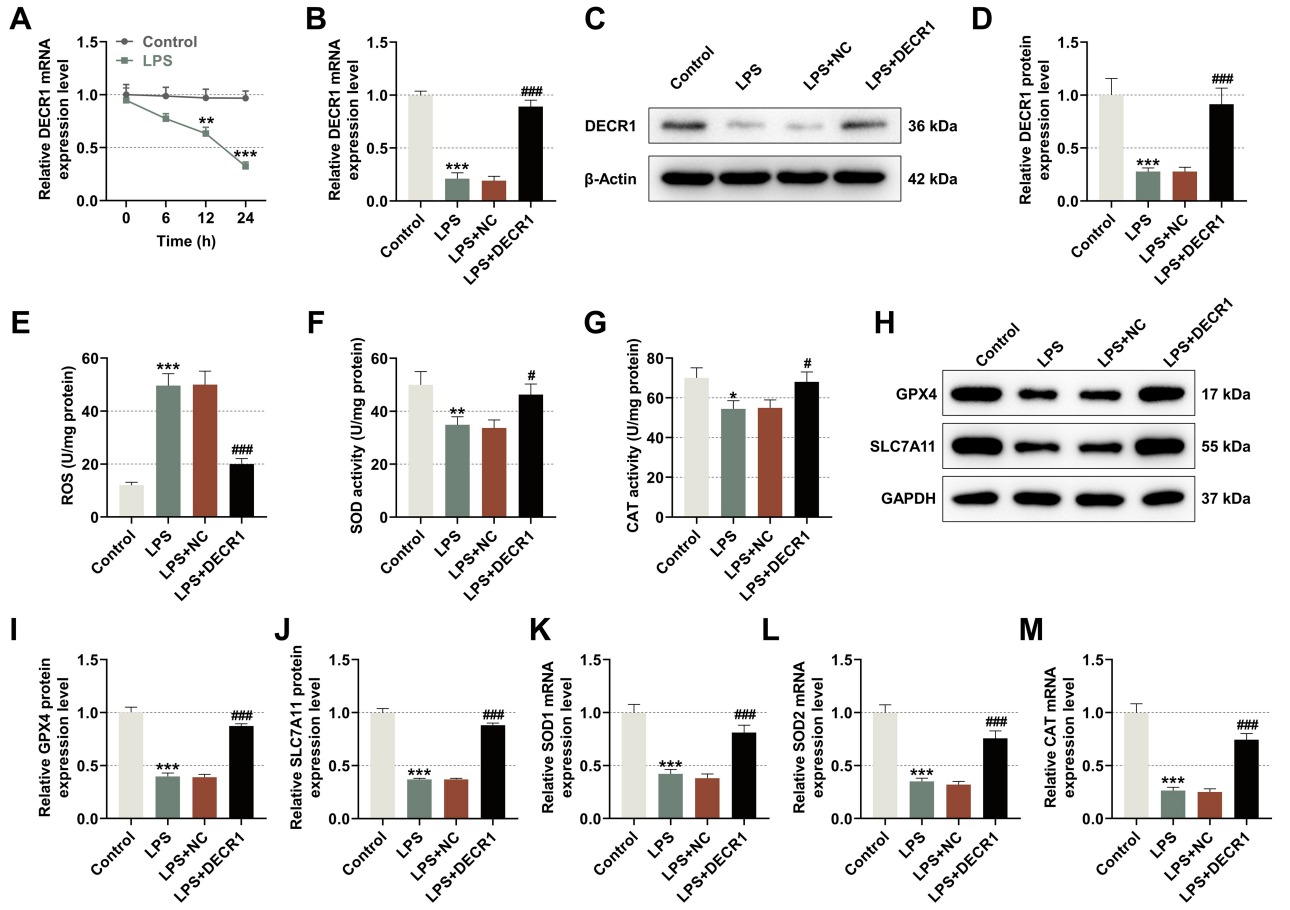

Fig. 5. *DECR1* overexpression dampened ferroptosis and enhanced antioxidant capability in LPS-exposed THP-1 cells. (A) *DECR1* expression was determined using qRT-PCR, with *GAPDH* and β-actin serving as internal reference genes. (B–D) THP-1 cells were exposed to 1 µg/mL LPS for 24 hours to induce septic MI after transfection with *DECR1* overexpression plasmids/NC. Subsequently, the expression levels of DECR1 in the cells were analyzed using qRT-PCR and Western blot analysis, with β-actin serving as internal references. (E–G) ROS, SOD, and CAT levels in the supernatant were determined using an enzyme-linked immunosorbent assay. (H–J) GPX4 and SLC7A11 expression levels were assessed in the cells using Western blot analysis, with GAPDH serving as an internal reference. (K–M) The expression levels of *SOD1*, *SOD2* and *CAT* in the cells were quantified using qRT-PCR, with *GAPDH* serving as an internal reference. One-way analysis of variance (ANOVA) was used for multiple group comparisons, followed by Tukey's post-hoc analysis, n = 3. $^{*}p < 0.05$, $^{**}p < 0.01$, $^{***}p < 0.001$ vs. Control group; $^{\#}p < 0.05$, $^{\#\#\#}p < 0.001$ vs. LPS+NC group. DECR1, 2,4-dienoyl-CoA reductase 1; MI, myocardial injury; NC, negative control; qRT-PCR, quantitative reverse transcription-polymerase chain reaction; GPX4, glutathione peroxidase 4; ROS, reactive oxygen species; SOD1/2, superoxidase dismutase 1/2; CAT, catalase.

Additionally, downregulation of GPX4, SLC7A11, SOD1, SOD2, and CAT was observed in LPS-stimulated THP-1 cells (Fig. 5H–M, $p < 0.001$); however, these effects were counteracted by *DECR1* overexpression (Fig. 5H–M, $p < 0.001$).

DECR1 Overexpression Abrogated LPS-induced Apoptosis and Inflammation in THP-1 Cells

Compared to the control cells, LPS-stimulated THP-1 cells showed decreased viability and an increased apoptosis rate (Fig. 6A–C, $p < 0.001$), accompanied by reduced Bcl-2 and elevated Bax and Cleaved Caspase 3 levels (Fig. 6D–G, $p < 0.001$). However, these LPS-induced effects were reversed by *DECR1* overexpression, restoring viability, Bcl-2 levels and decreasing apoptosis, Bax and Cleaved Caspase 3 expression (Fig. 6A–G, $p < 0.01$).

Additionally, LPS treatment increased the expression levels of IL-1β, IL-6, and TNF-α in cell supernatants (Fig. 6H–J, $p < 0.001$), while *DECR1* overexpression substantially decreased these inflammatory cytokines (Fig. 6H–J, $p < 0.001$). Similarly, LPS stimulation increased CRP and PCT levels in the supernatant of THP-1 cells (Fig. 6K,L, $p < 0.001$); however, this effect was attenuated by *DECR1* overexpression (Fig. 6K,L, $p < 0.001$).

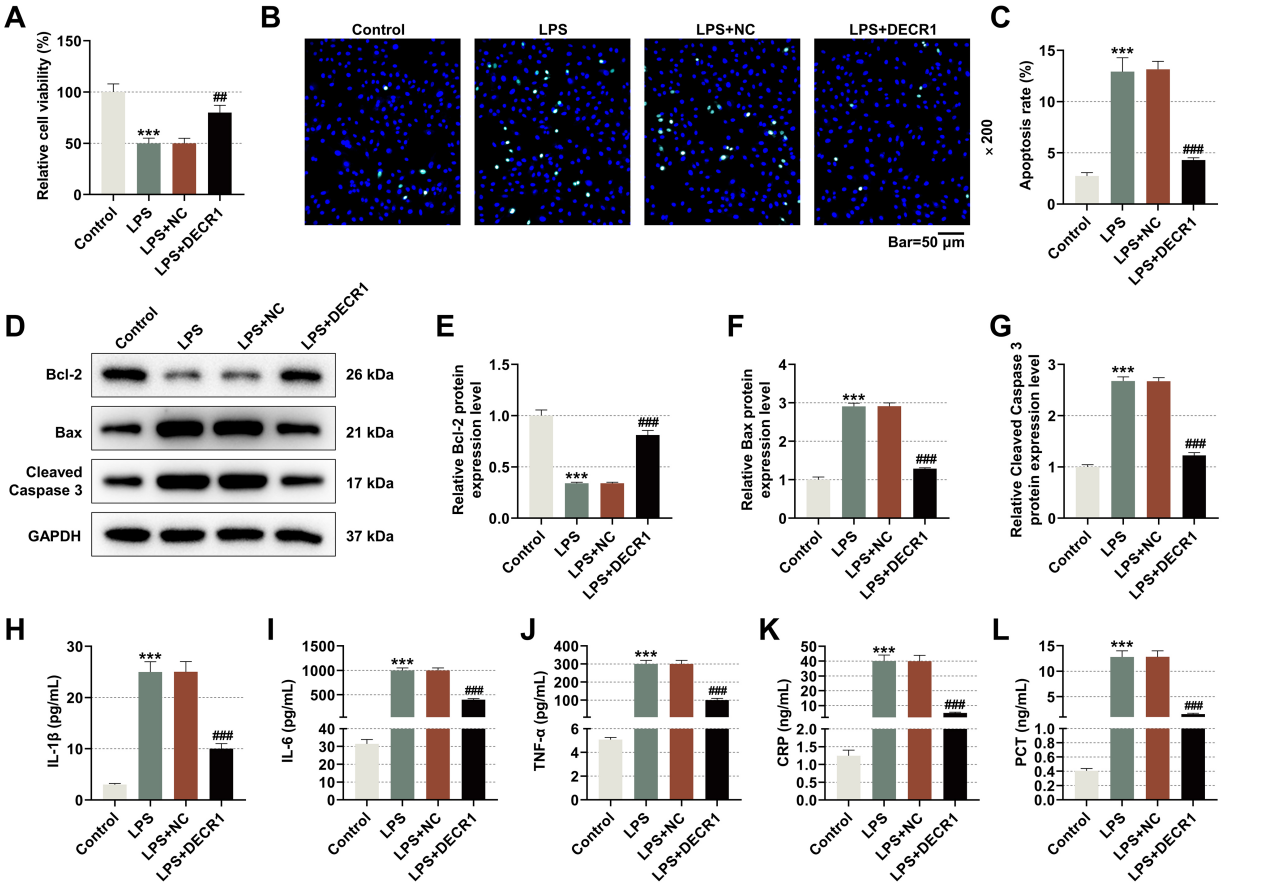

Fig. 6. *DECR1* overexpression abrogated LPS-induced apoptosis and inflammation in THP-1 cells. (A) THP-1 cells were transfected with *DECR1* overexpression plasmids/NC and then treated with 1 μg/mL LPS for 24 hours to induce septic MI. Thereafter, the cell viability was assessed using the cell counting kit8 assay. (B,C) The cell apoptosis was evaluated using TUNEL staining (magnification, ×200; scale bar, 50 μm). (D–G) Bcl-2, Bax, and Cleaved Caspase 3 expression levels were analyzed using Western blot analysis, with GAPDH serving as an internal reference. (H–J) IL-1β, IL-6, and TNF-α levels in the supernatant were determined using an enzyme-linked immunosorbent assay. (K,L) CRP and PCT levels were measured using a fluorescent immunoassay. One-way analysis of variance (ANOVA) was used for multiple group comparisons, followed by Tukey's post-hoc analysis, n = 3. $^{***}p < 0.001$ vs. Control group; $^{\#\#}p < 0.01$, $^{\#\#\#}p < 0.001$ vs. LPS+NC group. DECR1, 2,4-dienoyl-CoA reductase 1; MI, myocardial injury; NC, negative control; Bcl-2, B-cell lymphoma 2; Bax, Bcl-2-associated X protein; IL-1β, interleukin-1β; IL-6, interleukin-6; TNF-α; tumor necrosis factor-α; CRP, C-reactive protein; PCT, procalcitonin.

Discussion

Septic MI is associated with a decline in LVEF, which contributes to LV dilatation and perfusion failure as a maladaptive response, ultimately resulting in LV dysfunction and a substantial reduction in cardiac output (CO) [27]. Given the close link between MI complications and increased morbidity and mortality in septic patients [27], developing effective treatment approaches is crucial. Our study revealed that PBMC-derived DECR1 alleviates septic MI by suppressing inflammatory macrophage activation through the inhibition of macrophage ferroptosis.

In septic MI, inflammatory responses drive the overproduction of ROS, resulting in oxidative stress [4]. Mitochondria, through the electron transport chain (ETC), inherently generate ROS as byproducts; however, excessive ROS accumulation impairs mitochondrial function, which in turn exacerbates ETC-derived ROS production, thereby establishing a self-perpetuating cycle of oxidative stress [28,29]. DECR1, a mitochondria-related protein, participates in an auxiliary pathway for PUFA β-oxidation in eukaryotic mitochondria [14]. This indicates that DECR1 may affect oxidative stress in PBMCs during septic MI, thereby influencing the pathological condition of septic MI. Bioinformatics analyses predict a potential interaction between DECR1 and CAT. CAT is a heme enzyme that detoxifies hydrogen peroxide into water and oxygen; its inhibition reduces antioxidant capacity, leading to increased hydrogen peroxide levels [30]. CAT and the antioxidant enzyme SOD are important components of the endogenous

antioxidant system, and dysfunction of either enzyme leads to uncontrolled oxidative stress [31]. Precious studies show that CAT overexpression reduces the LPS-induced oxidative stress in cardiomyocytes [32] and attenuates oxidative stress and cardiac dysfunction in septic rodent models [33]. Consistent with these observations, our study revealed that overexpression of DECR1 inhibits ROS overproduction and restores CAT and SOD activities, thereby reducing oxidative stress in the myocardial tissues of septic MI rats.

Moreover, CAT has been found to mitigate LPS-induced cardiac dysfunction by mediating ferroptosis [32]. Ferroptosis is a distinct form of programmed cell death driven by iron and lipid hydroperoxide, which plays a crucial role in septic MI by targeting both cardiomyocytes and macrophages [8,34]. GPX4, a vital phospholipid hydroperoxidase, functions as an upstream regulator of ferroptosis by converting highly reactive lipid hydroperoxides into non-reactive lipid alcohols, thereby maintaining redox homeostasis and protecting cells from membrane lipid peroxidation [35,36]. Inhibition of GPX4 disrupts the antioxidant system, causing accumulation of lipid hydroperoxides and inducing ferroptosis [37].

The cystine/glutamate reverse transporter system x_c^- is comprised in part by SLC7A11, facilitates cystine uptake in exchange for glutamate export, thereby supporting glutathione (GSH) production and GPX4 activation, ultimately preventing ferroptosis [36]. In contrast, suppressing system x_c^- depletes GHS, inactivates GPX4, and triggers oxidative glutamate toxicity, lipid peroxidation, and subsequent ferroptosis [38]. Furthermore, DECR1 has been found to protect tumor cells from ferroptosis by impeding PUFA accumulation [16]. In line with the anti-ferroptotic role, our findings unveiled that DECR1 overexpression restores GPX4 and SLC7A11 levels in the myocardial tissues of septic MI rats, thereby reducing ferroptosis.

In septic MI, ferroptosis is strongly associated with reduced antioxidant capacity [38], as it interacts with and is induced by oxidative stress [39]. Consistently, we identified DECR1 overexpression elevated CAT, SOD1 and SOD2 mRNA expressions, accompanied by the ferroptosis inhibition in *in vivo* septic MI. Given that CAT can reduce ferroptosis and thereby mitigate cardiac injury [32], we suggest that DECR1 exerts an anti-ferroptotic role in septic MI by enhancing CAT activity through the upregulation of CAT mRNA expression. Moreover, targeting ferroptosis reduces myocardial inflammation, mitochondrial dysfunction, and cardiomyocyte apoptosis, ultimately improving cardiac performance, especially in alleviating LV dysfunction during sepsis [38,40].

The progression of septic MI is supported by inflammatory responses, which are amplified by the activation of macrophages that secrete pro-inflammatory chemokines [41]. In our study, downregulation of the PBMC-derived DECR1 was associated with elevated TNF-α, IL-1β, and IL-6 levels, along with increased contents of MI-related markers (TNI, HFABP, and ProBNP) [42,43] and myocarditis-related markers (CRP and PCT) [44]. Collectively, these results highlight that DECR1 deficiency in PBMCs plays a crucial role in the progression of septic MI.

Furthermore, we proposed that DECR1 downregulation in septic MI-derived PBMCs induces ferroptosis in macrophages, thereby facilitating their pro-inflammatory activation and accelerating disease progression. Given that LPS is an immunomodulator known to induce macrophage polarization that can secrete pro-inflammatory cytokines, including IL-1β, IL-6, and TNF-α [41], our study examined this pathway *in vitro*. Our *in vitro* experiments confirmed that DECR1 suppresses oxidative stress by activating CAT, thereby reducing ferroptosis, which is translatable in LPS-induced THP-1 cells. Because ferroptosis induction commonly represses GPX4 expression, it contributes to mitochondrial dysfunction-induced apoptosis in septic MI [39]. Apoptosis of macrophages further exacerbates the inflammatory response during early sepsis [45], whereas excessive macrophage apoptosis in late-stage sepsis leads to immunosuppression and organ injury, aggravating infection severity [46]. Our study revealed that DECR1 overexpression inhibited LPS-induced apoptosis and ferroptosis of THP-1 cells, while reducing the secretion of pro-inflammatory cytokines and myocarditis-related markers. These results indicate that DECR1 protects against macrophage apoptosis and pro-inflammatory activation by dampening ferroptosis of macrophages, thereby potentially reducing the progression of septic MI.

Mechanistically, membrane lipid peroxidation results in the release of cytochrome C, inducing Caspase 3-dependent apoptosis, characterized by the downregulation of the antiapoptotic protein Bcl-2 and the upregulation of the pro-apoptotic protein Bax. As demonstrated, in septic MI, increased GPX4 levels protect mitochondria against this peroxidative damage [39,47]. Additionally, previous research has revealed that oxidative stress-induced ferroptosis combined with apoptotic inhibition can help maintain long-term cellular homeostasis [48].

Therefore, we further investigated apoptosis and demonstrated that DECR1 overexpression inhibits apoptosis, as evidenced by increased Bcl-2 expression and decreased Bax and Cleaved Caspase 3 expressions. It is worth noting that the loss of Bcl-2 not only promotes apoptosis but may also trigger ferroptosis by inactivating GPX4 [49]. In contrast, other studies have reported that overexpression of Bcl-2 alleviates ferroptosis induced by excessive molybdenum and cadmium by reducing mitochondrial ROS levels in duck kidneys [50]. These findings suggest that there may be complex interactions between apoptosis-related molecules (such as Bcl-2 and Bax) and ferroptosis regulators (such as GPX4), highlighting a close link between apoptosis and ferroptosis. In support of this, LINC00618 has been found to accelerate ferroptosis via apoptosis [51].

However, we must candidly acknowledge a limitation of our study: although this study provides indirect evidence of the association between ferroptosis and apoptosis based on molecular expression changes (such as GPX4, Bcl-2/Bax, Caspase 3, etc.), this analysis lacked the advanced technical tools, such as the dual fluorescence reporter system, to directly visualize and quantitatively verify ferroptosis and apoptosis within the same cells. Therefore, future studies should focus on elucidating the potential association and cross-regulation between apoptosis and ferroptosis to enhance the understanding of the mechanism under myocardial injury in sepsis. Such investigations could provide a solid theoretical basis and potential therapeutic targets for managing MI in septic patients.

We also acknowledge some other limitations in our study. First, our experimental techniques did not allow for the specific overexpression of DECR1 in PBMCs at the beginning of the modeling, which may limit the reliability that the observed inhibition of septic MI is attributed to DECR1 derived from PBMCs. Second, we did not conduct validation experiments using DECR1 knockout or silencing models, and our results are currently based solely on animal and cell models. Additionally, assessing cardiac function relied solely on echocardiographic indicators (LVEF, LVFS), and further investigations are needed to validate the clinical significance of these findings. Future studies should incorporate more designed approaches, such as C11-BODIPY staining and Annexin V/PI flow cytometry, to verify these findings once current technical limitations are addressed. Furthermore, comprehensive molecular investigations are required to explore the downstream pathways and ferroptosis mechanisms regulated by DECR1, as well as to examine the crucial role of macrophage-secreted inflammatory factors and the relationship between DECR1 and other antioxidant proteins.

Conclusion

In conclusion, our study provides novel insights into the mechanism of PBMC-derived DECR1 in septic MI. Concretely, overexpression of PBMC-derived DECR1 inhibits ferroptosis in macrophages by activating CAT, thereby dampening myocardial inflammation and apoptosis while maintaining cardiac function by prolonging LVEDV and LVESV. These findings highlight that PBMC-derived DECR1 may serve as a valuable therapeutic target for the clinical management of septic MI.

Availability of Data and Materials

The datasets used and/or analyzed during the current study are available from the corresponding author upon reasonable request.

Author Contributions

WZ and JM designed the research study; WZ, ZL, JM and LP performed the research; LP, JM and MD collected and analyzed the data. WZ and JM have been involved in drafting and all authors have been involved in revising it critically for important intellectual content. All authors have read and approved the final manuscript. All authors have participated sufficiently in the work and agreed to be accountable for all aspects of the work.

Ethics Approval and Consent to Participate

All animal experiments were performed following the National Institutes of Health guidelines for the Animal Care and Use and were approved by the Ethics Committee for Experimental Animals Welfare of the Zhejiang Academy of Traditional Chinese Medicine (No. 034, 2023).

Acknowledgment

Not applicable.

Funding

This work was supported by Zhejiang Medicine and Health Science and Technology Project [grant number: 2022KY700], Zhejiang Medicine and Health Science and Technology Project [grant number: 2024KY879], Zhejiang Province Traditional Chinese Medicine Science and Technology Project [grant number: 2023ZL031] and Zhejiang Basic Public Welfare Project [grant number: LGF21H010003].

Conflict of Interest

The authors declare no conflict of interest.

Supplementary Material

Supplementary material associated with this article can be found, in the online version, at https://doi.org/10.24976/Discov.Med.202537201.195.

References

[1] Srzić I, Nesek Adam V, Tunjić Pejak D. SEPSIS DEFINITION: WHAT'S NEW IN THE TREATMENT GUIDELINES. Acta Clinica Croatica. 2022; 61: 67–72. https://doi.org/10.20471/acc.2022.61.s1.11.

[2] L'Heureux M, Sternberg M, Brath L, Turlington J, Kashiouris MG. Sepsis-Induced Cardiomyopathy: a Comprehensive Review. Current Cardiology Reports. 2020; 22: 35. https://doi.org/10.1007/s11886-020-01277-2.

[3] Liang YW, Zhu YF, Zhang R, Zhang M, Ye XL, Wei JR. Incidence, prognosis, and risk factors of sepsis-induced cardiomyopathy. World Journal of Clinical Cases. 2021; 9: 9452–9468. https://doi.org/10.12998/wjcc.v9.i31.9452.

[4] Carbone F, Liberale L, Preda A, Schindler TH, Montecucco F. Septic Cardiomyopathy: From Pathophysiology to the Clinical Setting. Cells. 2022; 11: 2833. https://doi.org/10.3390/cells11182833.

[5] Sansonetti M, Waleczek FJG, Jung M, Thum T, Perbellini F. Resident cardiac macrophages: crucial modulators of cardiac (patho)physiology. Basic Research in Cardiology. 2020; 115: 77. https://doi.org/10.1007/s00395-020-00836-6.

[6] Alvarez-Argote S, O'Meara CC. The Evolving Roles of Cardiac Macrophages in Homeostasis, Regeneration, and Repair. International Journal of Molecular Sciences. 2021; 22: 7923. https://doi.org/10.3390/ijms22157923.

[7] Zhang K, Wang Y, Chen S, Mao J, Jin Y, Ye H, *et al*. TREM2^{hi} resident macrophages protect the septic heart by maintaining cardiomyocyte homeostasis. Nature Metabolism. 2023; 5: 129–146. https://doi.org/10.1038/s42255-022-00715-5.

[8] Kong C, Ni X, Wang Y, Zhang A, Zhang Y, Lin F, *et al*. ICA69 aggravates ferroptosis causing septic cardiac dysfunction via STING trafficking. Cell Death Discovery. 2022; 8: 187. https://doi.org/10.1038/s41420-022-00957-y.

[9] Liu N, Liang Y, Wei T, Zou L, Huang X, Kong L, *et al*. The role of ferroptosis mediated by NRF2/ERK-regulated ferritinophagy in CdTe QDs-induced inflammation in macrophage. Journal of Hazardous Materials. 2022; 436: 129043. https://doi.org/10.1016/j.jhazmat.2022.129043.

[10] Chen XS, Wang SH, Liu CY, Gao YL, Meng XL, Wei W, *et al*. Losartan attenuates sepsis-induced cardiomyopathy by regulating macrophage polarization via TLR4-mediated NF-κB and MAPK signaling. Pharmacological Research. 2022; 185: 106473. https://doi.org/10.1016/j.phrs.2022.106473.

[11] Fang X, Wang H, Han D, Xie E, Yang X, Wei J, *et al*. Ferroptosis as a target for protection against cardiomyopathy. Proceedings of the National Academy of Sciences of the United States of America. 2019; 116: 2672–2680. https://doi.org/10.1073/pnas.1821022116.

[12] Gong CW, Yuan MM, Qiu BQ, Wang LJ, Zou HX, Hu T, *et al*. Identification and Validation of Ferroptosis-Related Biomarkers in Septic Cardiomyopathy via Bioinformatics Analysis. Frontiers in Genetics. 2022; 13: 827559. https://doi.org/10.3389/fgene.2022.827559.

[13] Long Q, Li G, Dong Q, Wang M, Li J, Wang L. Exploration of the Shared Gene Signatures between Myocardium and Blood in Sepsis: Evidence from Bioinformatics Analysis. BioMed Research International. 2022; 2022: 3690893. https://doi.org/10.1155/2022/3690893.

[14] Blomme A, Ford CA, Mui E, Patel R, Ntala C, Jamieson LE, *et al*. 2,4-dienoyl-CoA reductase regulates lipid homeostasis in treatment-resistant prostate cancer. Nature Communications. 2020; 11: 2508. https://doi.org/10.1038/s41467-020-16126-7.

[15] Sanchez-Ruderisch H, Queirós AM, Fliegner D, Eschen C, Kararigas G, Regitz-Zagrosek V. Sex-specific regulation of cardiac microRNAs targeting mitochondrial proteins in pressure overload. Biology of Sex Differences. 2019; 10: 8. https://doi.org/10.1186/s13293-019-0222-1.

[16] Nassar ZD, Mah CY, Dehairs J, Burvenich IJ, Irani S, Centenera MM, *et al*. Human DECR1 is an androgen-repressed survival factor that regulates PUFA oxidation to protect prostate tumor cells from ferroptosis. eLife. 2020; 9: e54166. https://doi.org/10.7554/eLife.54166.

[17] Wang L, Zhang Y, Yu M, Yuan W. Identification of Hub Genes in the Remodeling of Non-Infarcted Myocardium Following Acute Myocardial Infarction. Journal of Cardiovascular Development and Disease. 2022; 9: 409. https://doi.org/10.3390/jcdd9120409.

[18] Percie du Sert N, Hurst V, Ahluwalia A, Alam S, Avey MT, Baker M, *et al*. The ARRIVE guidelines 2.0: Updated guidelines for reporting animal research. PLoS Biology. 2020; 18: e3000410. https://doi.org/10.1371/journal.pbio.3000410.

[19] Yang C, Xia W, Liu X, Lin J, Wu A. Role of TXNIP/NLRP3 in sepsis-induced myocardial dysfunction. International Journal of Molecular Medicine. 2019; 44: 417–426. https://doi.org/10.3892/ijmm.2019.4232.

[20] Liu JJ, Li Y, Yang MS, Chen R, Cen CQ. SP1-induced ZFAS1 aggravates sepsis-induced cardiac dysfunction via miR-590-3p/NLRP3-mediated autophagy and pyroptosis. Archives of Biochemistry and Biophysics. 2020; 695: 108611. https://doi.org/10.1016/j.abb.2020.108611.

[21] Zeng Y, Cao G, Lin L, Zhang Y, Luo X, Ma X, *et al*. Resveratrol Attenuates Sepsis-Induced Cardiomyopathy in Rats through Anti-Ferroptosis via the Sirt1/Nrf2 Pathway. Journal of Investigative Surgery: the Official Journal of the Academy of Surgical Research. 2023; 36: 2157521. https://doi.org/10.1080/08941939.2022.2157521.

[22] Riedhammer C, Halbritter D, Weissert R. Peripheral Blood Mononuclear Cells: Isolation, Freezing, Thawing, and Culture. Methods in Molecular Biology (Clifton, N.J.). 2016; 1304: 53–61. https://doi.org/10.1007/7651_2014_99.

[23] Cai J, Lu S, Yao Z, Deng YP, Zhang LD, Yu JW, *et al*. Glibenclamide attenuates myocardial injury by lipopolysaccharides in streptozotocin-induced diabetic mice. Cardiovascular Diabetology. 2014; 13: 106. https://doi.org/10.1186/s12933-014-0106-y.

[24] Lendoiro-Cino N, Rodríguez-Coello A, Saborido A, F-Burguera E, Fernández-Rodríguez JA, Meijide-Faílde R, *et al*. Study of hydrogen sulfide biosynthesis in synovial tissue from diabetes-associated osteoarthritis and its influence on macrophage phenotype and abundance. Journal of Physiology and Biochemistry. 2023; 79: 653–667. https://doi.org/10.1007/s13105-023-00968-y.

[25] Livak KJ, Schmittgen TD. Analysis of relative gene expression data using real-time quantitative PCR and the 2(-Delta Delta C(T)) Method. Methods (San Diego, Calif.). 2001; 25: 402–408. https://doi.org/10.1006/meth.2001.1262.

[26] Zhu Y, Zhang X, Yang K, Shao Y, Gu R, Liu X, *et al*. Macrophage-derived apoptotic vesicles regulate fate commitment of mesenchymal stem cells via miR155. Stem Cell Research & Therapy. 2022; 13: 323. https://doi.org/10.1186/s13287-022-03004-w.

[27] Hollenberg SM, Singer M. Pathophysiology of sepsis-induced cardiomyopathy. Nature Reviews. Cardiology. 2021; 18: 424–434. https://doi.org/10.1038/s41569-020-00492-2.

[28] Bi CF, Liu J, Yang LS, Zhang JF. Research Progress on the Mechanism of Sepsis Induced Myocardial Injury. Journal of Inflammation Research. 2022; 15: 4275–4290. https://doi.org/10.2147/JIR.S374117.

[29] Liu S, Chong W. Roles of LncRNAs in Regulating Mitochondrial Dysfunction in Septic Cardiomyopathy. Frontiers in Immunology. 2021; 12: 802085. https://doi.org/10.3389/fimmu.2021.802085.

[30] Gebicka L, Krych-Madej J. The role of catalases in the prevention/promotion of oxidative stress. Journal of Inorganic Biochemistry. 2019; 197: 110699. https://doi.org/10.1016/j.jinorgbio.2019.110699.

[31] Poprac P, Jomova K, Simunkova M, Kollar V, Rhodes CJ, Valko M. Targeting Free Radicals in Oxidative Stress-Related Human Diseases. Trends in Pharmacological Sciences. 2017; 38: 592–607. https://doi.org/10.1016/j.tips.2017.04.005.

[32] Peng H, Zhang J, Zhang Z, Turdi S, Han X, Liu Q, *et al*. Cardiac-specific overexpression of catalase attenuates lipopolysaccharide-induced cardiac anomalies through reconciliation of autophagy and ferroptosis. Life Sciences. 2023; 328: 121821. https://doi.org/10.1016/j.lfs.2023.121821.

[33] Haileselassie B, Su E, Pozios I, Niño DF, Liu H, Lu DY, *et al*. Myocardial oxidative stress correlates with left ventricular dysfunction on strain echocardiography in a rodent model of sepsis. Intensive Care Medicine Experimental. 2017; 5: 21. https://doi.org/10.1186/s40635-017-0134-5.

[34] Li N, Wang W, Zhou H, Wu Q, Duan M, Liu C, *et al*. Ferritinophagy-mediated ferroptosis is involved in sepsis-induced cardiac injury. Free Radical Biology & Medicine. 2020; 160: 303–318. https://doi.org/10.1016/j.freeradbiomed.2020.08.009.

[35] Agmon E, Stockwell BR. Lipid homeostasis and regulated cell death. Current Opinion in Chemical Biology. 2017; 39: 83–89. https://doi.org/10.1016/j.cbpa.2017.06.002.

[36] Chen X, Li J, Kang R, Klionsky DJ, Tang D. Ferroptosis: machinery and regulation. Autophagy. 2021; 17: 2054–2081. https://doi.org/10.1080/15548627.2020.1810918.

[37] Forcina GC, Dixon SJ. GPX4 at the Crossroads of Lipid Homeostasis and Ferroptosis. Proteomics. 2019; 19: e1800311. https://doi.org/10.1002/pmic.201800311.

[38] Cao G, Zeng Y, Zhao Y, Lin L, Luo X, Guo L, *et al*. H2S regulation of ferroptosis attenuates sepsis induced cardiomyopathy. Molecular Medicine Reports. 2022; 26: 335. https://doi.org/10.3892/mmr.2022.12851.

[39] Ren JX, Li C, Yan XL, Qu Y, Yang Y, Guo ZN. Crosstalk between Oxidative Stress and Ferroptosis/Oxytosis in Ischemic Stroke: Possible Targets and Molecular Mechanisms. Oxidative Medicine and Cellular Longevity. 2021; 2021: 6643382. https://doi.org/10.1155/2021/6643382.

[40] Sun H, Chen D, Xin W, Ren L, Li Q, Han X. Targeting ferroptosis as a promising therapeutic strategy to treat cardiomyopathy. Frontiers in Pharmacology. 2023; 14: 1146651. https://doi.org/10.3389/fphar.2023.1146651.

[41] Facchin BM, Dos Reis GO, Vieira GN, Mohr ETB, da Rosa JS, Kretzer IF, *et al*. Inflammatory biomarkers on an LPS-induced RAW 264.7 cell model: a systematic review and meta-analysis. Inflammation Research: Official Journal of the European Histamine Research Society ... [et al.]. 2022; 71: 741–758. https://doi.org/10.1007/s00011-022-01584-0.

[42] Jeong JH, Seo YH, Ahn JY, Kim KH, Seo JY, Kim MJ, *et al*. The Prognostic Value of Serum Levels of Heart-Type Fatty Acid Binding Protein and High Sensitivity C-Reactive Protein in Patients With Increased Levels of Amino-Terminal Pro-B Type Natriuretic Peptide. Annals of Laboratory Medicine. 2016; 36: 420–426. https://doi.org/10.3343/alm.2016.36.5.420.

[43] Mehta NJ, Khan IA, Gupta V, Jani K, Gowda RM, Smith PR. Cardiac troponin I predicts myocardial dysfunction and adverse outcome in septic shock. International Journal of Cardiology. 2004; 95: 13–17. https://doi.org/10.1016/j.ijcard.2003.02.005.

[44] Rehman A, Yousuf S, Maken GR, Naqvi SRA, Murtaza G, Ahmad A. Cardiac Troponin-I, A Biomarker for Predicting COVID-Induced Myocardial Damage Prognosis. Journal of the College of Physicians and Surgeons–Pakistan: JCPSP. 2023; 33: 498–503. https://doi.org/10.29271/jcpsp.2023.05.498.

[45] Wen X, Xie B, Yuan S, Zhang J. The "Self-Sacrifice" of ImmuneCells in Sepsis. Frontiers in Immunology. 2022; 13: 833479. https://doi.org/10.3389/fimmu.2022.833479.

[46] Qiu P, Liu Y, Zhang J. Review: the Role and Mechanisms of Macrophage Autophagy in Sepsis. Inflammation. 2019; 42: 6–19. https://doi.org/10.1007/s10753-018-0890-8.

[47] Xu P, Zhang WQ, Xie J, Wen YS, Zhang GX, Lu SQ. Shenfu injection prevents sepsis-induced myocardial injury by inhibiting mitochondrial apoptosis. Journal of Ethnopharmacology. 2020; 261: 113068. https://doi.org/10.1016/j.jep.2020.113068.

[48] Wang GX, Tu HC, Dong Y, Skanderup AJ, Wang Y, Takeda S, *et al*. ΔNp63 Inhibits Oxidative Stress-Induced Cell Death, Including Ferroptosis, and Cooperates with the BCL-2 Family to Promote Clonogenic Survival. Cell Reports. 2017; 21: 2926–2939. https://doi.org/10.1016/j.celrep.2017.11.030.

[49] Setiawan SA, Liu WZ, Weng PW, Lee CH, Yadav VK, Hardianti MS, *et al*. Synergistic disruption of BTK and BCL-2 causes apoptosis while inducing ferroptosis in double-hit lymphoma. European Journal of Pharmacology. 2023; 943: 175526. https://doi.org/10.1016/j.ejphar.2023.175526.

[50] Liu H, Zhang C, Li S, Wang S, Xiao L, Chen J, *et al*. Overexpression Bcl-2 alleviated ferroptosis induced by molybdenum and cadmium co-exposure through inhibiting mitochondrial ROS in duck kidneys. International Journal of Biological Macromolecules. 2025; 291: 139118. https://doi.org/10.1016/j.ijbiomac.2024.139118.

[51] Wang Z, Chen X, Liu N, Shi Y, Liu Y, Ouyang L, *et al*. A Nuclear Long Non-Coding RNA LINC00618 Accelerates Ferroptosis in a Manner Dependent upon Apoptosis. Molecular Therapy: the Journal of the American Society of Gene Therapy. 2021; 29: 263–274. https://doi.org/10.1016/j.ymthe.2020.09.024.